第 489 回電波研連 F 分科会
開催日: 2004 年 11 月 19 日

Co-Polarization Measurements for Ultra Wideband Double-Directional Channel Characterization

Hiroaki TSUCHIYA, Katsuyuki HANEDA, Jun-ichi TAKADA
Department of International Development Engineering, Tokyo Institute of Technology
S6-4, 2-12-1, O-okayama, Meguro-ku, Tokyo 152-8550, Japan
Email: tutiya@ap.ide.titech.ac.jp

Abstract

In this paper, the double-directional channel measurement and spatio-temporal analysis of UWB propagation based on the clusterization approach were reported. After separating the deterministic and diffuse components both on transmit (Tx) and Receive (Rx) positions, the deterministic components both on Tx and Rx positions are observed for some clusters separately, while coupling the clusters between Tx and Rx position based on similar time of arrivals (ToAs), and ray tracing by utilizing high temporal and spatio resolution, respectively. Then the relation between direction of departure (DoD) and direction of arrival (DoA) will be investigated. For intra-cluster properties, they were derived based on the moment analysis, and their characteristics were discussed. Finally, a comparison of V-V and H-H polarization are shown.

Keywords : Ultra Wideband, UWB, double directional, channel model, propagation, scattering, clusterization, reflection, characterization

1 Introduction

Recently, ultra-wideband (UWB) radio has been attracting attention due to their ability to provide high data rates, extreme low power and high resolution for indoor wireless communications. However, its system performance can suffer from dense multipath propagation. So it is required to investigate the propagation channel where the system is to be implemented. For elucidating the propagation channels of UWB indoor multipath environments, we have already proposed a frequency domain channel estimation scheme in a deterministic way which achieves high resolution with an UWB signal [1], [2], [3]. It is also important to decouple the antenna and channel characteristics in the UWB channel model for evaluation of antenna systems, because every antenna has its original characteristics and it is not flat in the frequency domain. This paper shows the results of double-directional [4] channel characterization in the spatio-temporal domain. It is necessary to decouple the transmit (Tx), Receive (Rx) antennas and channel characteristics for every multipath. By first detecting the waves from both the Tx and Rx spatial sampling data, and separating deterministic components and diffuse components. Then, clusterization of deterministic components was conducted by using both direction of departure (DoD) and direction of arrival (DoA). Comparing the clusters of DoD and DoA, we found most clusters can be coupled to the physical phenomena with its intra-cluster properties. Several qualitative observations are also given.

2 Measurement Setup

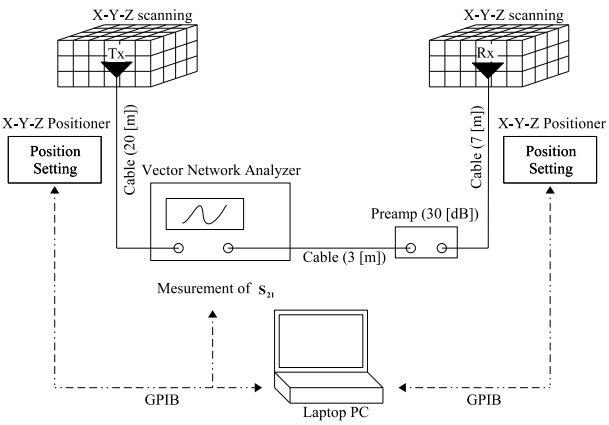

Figure 1: UWB double-directional channel sounding system

Table 1: Specifications of the experiment

Bandwidth	3.1 to 10.6 [GHz]
Frequency sweeping points	751
Spatial sampling in the Rx and Tx position	$10 \times 10 \times 7$ points in X-Y-Z whose element spacing is 48 [mm] (less than half wavelength at 3.1 [GHz])
Estimated parameters	DoD and DoA azimuth, elevation angle, delay time, and spectrum.
Type of antennas	Biconical [5]
Polarization	Vertical-Vertical (V-V), Horizontal-Horizontal (H-H)
Calibration	Function of VNA and back-to-back
IF bandwidth of VNA	100 [Hz]
Sub-bandwidth	3 [GHz]

Figure 1 shows the UWB double-directional channel sounding system. The measurements have been performed with a vector network analyzer (VNA) to determine the complex radio channel transfer function $H(f) = S_{21}(f)$. Some indispensable parameters are shown in Table 1. First, the Tx antenna was mounted on a tripod and its position was fixed at the center of the array, while the Rx antenna was mounted on the arm of the X-Y-Z scanner to measure the DoA. After the scanning of Rx was finished, we scanned the opposite side to measure the DoD, while fixing Rx at the center of the array. In the measurements, the element spacing of the synthesized array was set to 48 [mm], which was equivalent to 0.49λ at the lowest frequency. All processes were controlled automatically by the GPIB, as well as the data acquisition. The measurement was performed in an empty office room, with no furniture. The spherical wave array mode vector was adopted because it is better for indoor propagation compared to the plane wave model [2]. We measured 700 spatial samples in both scanning areas. Figure 2 shows the layout of the measurement environment. Note that the azimuth angle is defined with respect to the line-of-sight (LOS), and is opposite for the Tx and Rx sides.

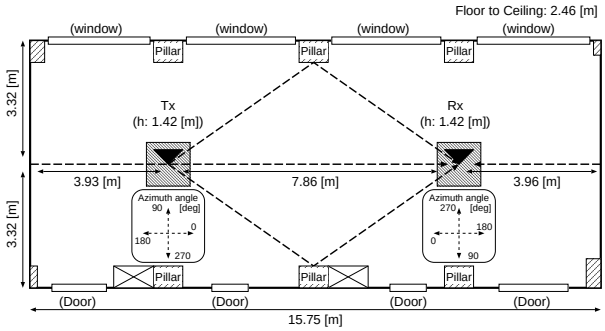

(a) Top view

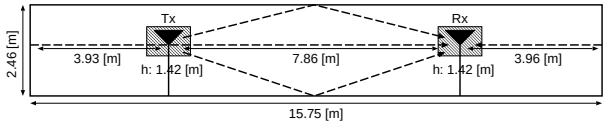

(b) Side view

Figure 2: The experiment environment

3 Data Processing and Analysis

From the measurement data, the parameters and spectrum of each wave were estimated using the SAGE algorithm that is based on the deterministic approach of propagation channel characterization. It was implemented with the Successive Interference Cancellation (SIC) [6] process. Details of the algorithm can be found in Refs [1], [2]. DoDs and DoAs are estimated separately by using two single-directional channel measurements, and they are related by using high resolution time of arrival (ToA) and ray tracing. This is because the spherical wave model and double-directional model are incompatible. The spherical wave model assumes that the signal comes from a point source while the double directional model considers that the signal is coming from a widely distributed source because both sides uses multiple antennas resulting in multiple sources which cannot be assumed as coming from one single source.

For convenience, the analysis of V-V polarization is shown first, and then its difference with H-H polarization is shown next.

3.1 Separation of Deterministic and Diffuse Components

Figures 3 and 4 show the azimuth-delay power spectrum at TX and RX respectively. The direct wave appears near position $(0, 27)$, and also its side-

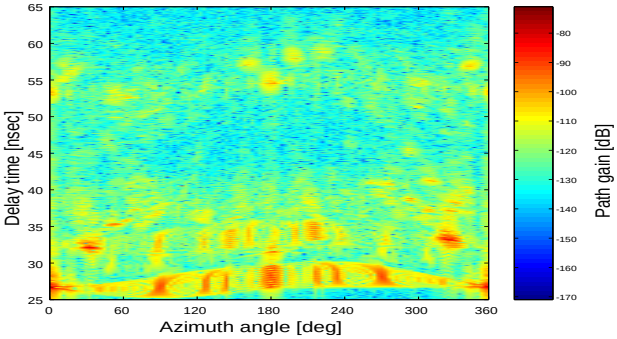

(a) Total power spectrum

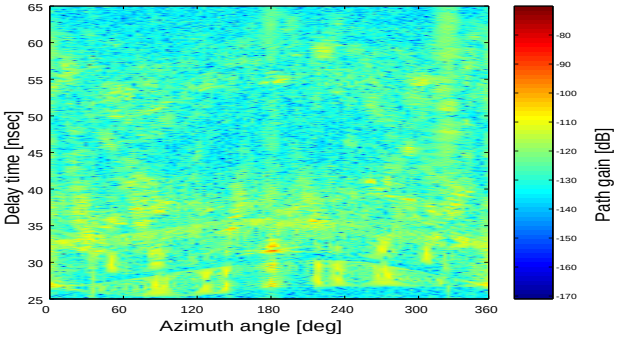

(b) Residual spectrum after the extraction of 120 waves

Figure 3: Azimuth - delay power spectrum at Tx (V-V)

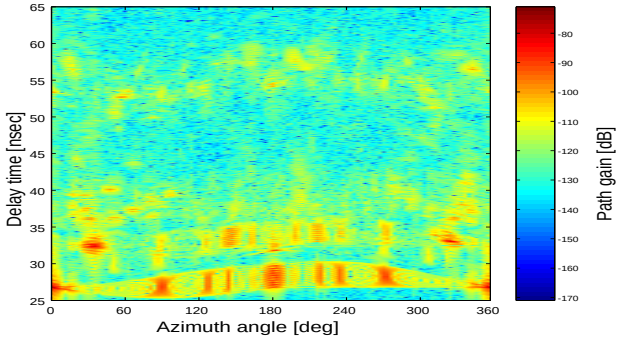

(a) Total power spectrum

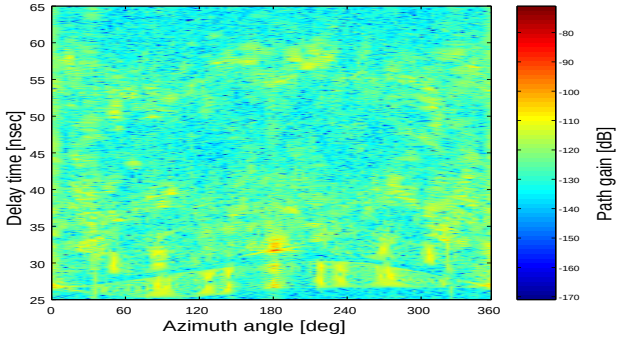

(b) Residual spectrum after the extraction of 120 waves

Figure 4: Azimuth - delay power spectrum at Rx (V-V)

lobe appears between delay time $y(25)$ to $y(30)$ at all azimuth angles. But SAGE algorithm is able to distinguish them. To separate the deterministic and diffuse components, we should calculate the noise floor. According to the VNA, the noise floor level was shown to be -100 to -90 [dB], but we measured a total of 700 spatial samples and 751 frequency sweeping points, so the noise floor level should be lower by $|-10\log_{10}(700\times751)| \simeq 57$ [dB]. We detected 120 waves each at Tx and Rx positions, and regard them as deterministic components, while the residuals were considered as diffuse components. The power of the detected waves at the Tx position was comparable with that at the Rx position according to Fig. 5. But the percentage of the sum of the extracted power are different. The deterministic components at Tx position consist of about 65%, while at the other position, it consists of about 73% of the total power, as shown in Fig. 6. The total power is -66.85 [dB] and -66.38 [dB] at Tx and Rx positon respectively, but for line of sight (LOS), there are some errors between Tx and Rx position (The value of LOS can be found in Tables 2 and 3). These errors are probably due to the antenna setting. In other experiments e.g. [3], [7], the deterministic components consisted of about 70% and 90% respectively by using the same algorithm.

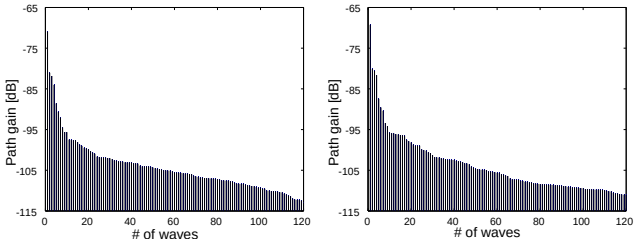

(a) Tx position (b) Rx position

Figure 5: Power of each detected wave (V-V)

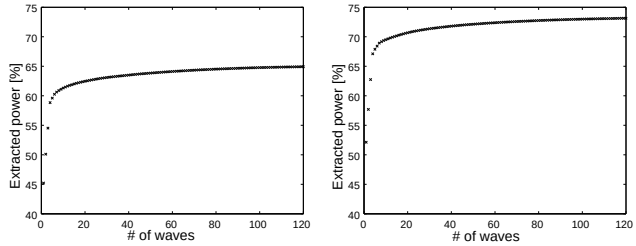

(a) Tx position (b) Rx position

Figure 6: Percentage of the sum of the extracted power (V-V)

3.2 Clusterization of Deterministic Components

Figures 7 and 8 show the extracted deterministic components in angular-delay domains at Tx and

Rx positions respectively. These results show that the detected waves tend to form some clusters in the spatio-temporal domain. We define a cluster as an accumulation of detected waves with similar ToAs and DoDs for the Tx position and similar ToAs and DoAs for the Rx position. Moreover, the clusters are related to the physical structures of the experiment environment i.e., specular reflection, material, position and size of reflection objects, using a heuristic approach. In the statistical model, the mean value is more important than the maximum value. But for the deterministic model, both are important. The parameters of the wave with the maximum power in each cluster are shown in Tables 2 and 3. For intra-cluster properties, we show the mean and spread of estimated parameters in Tables 4 and 5.

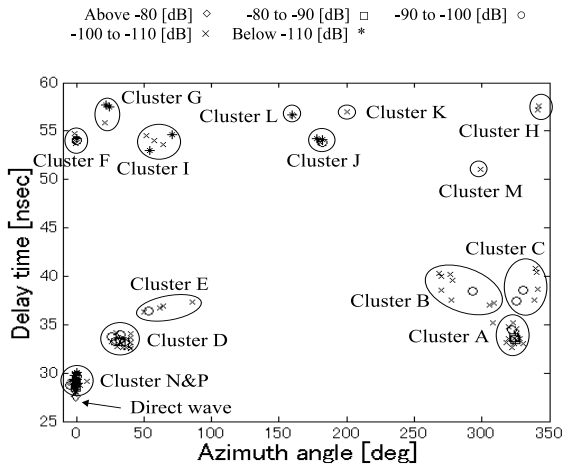

Figure 7: Clusterization of deterministic components at Tx (V-V)

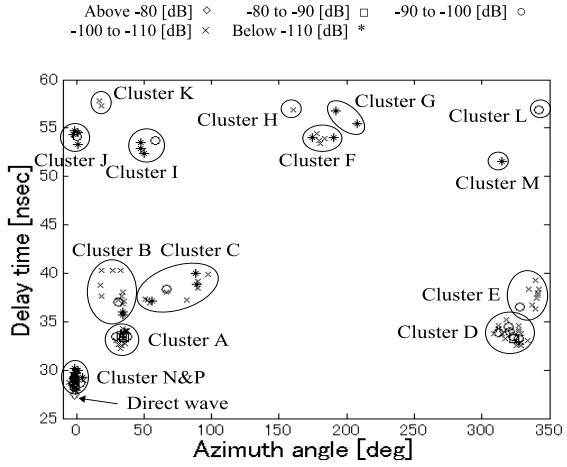

Figure 8: Clusterization of deterministic components at Rx (V-V)

3.3 Coupling the clusters between the Tx and Rx position

In order to understand the relation between the Tx and Rx position, we coupled the clusters between the Tx and Rx position based on delay time and ray tracing. We then see that all clusters can be coupled and thus are given the same name in both sides. The identification of these clusters are shown in Fig. 15. There are some errors in the delay time and path gain by comparing Tables 2 and 3. This is due to the approximation of the double directional measurement by using two single directional measurements as mentioned above. This is also true for Tables 4 and 5.

Clusters A and D consist of scattering from the pillars. Some waves have high power values in these clusters. Clusters B, C and E consist of scattering from the pillars, metal doors and window frames. The angular spread not near the Tx and Rx position depend on the location of the refection. Clusters F and J consist of scattering from the walls. The power of these clusters are low. Clusters G, H, I, K, L and M consist of scattering from the pillars, metal doors, window frames and walls. These clusters also have close relation in the DoDs and DoAs. Because all of these clusters have long delay times, means these waves are not only scattered by a single object. Note that the relation of these clusters can only be investigated by using double-directional channel measurements. Clusters N and P consist of scattering waves at the ceiling and floor respectively. Although the delay times of these clusters are short, the waves in each cluster can be separated by their DoDs and DoAs.

Table 2: Parameters of the wave with the maximum power in the Tx position clusters (V-V)

Cluster	Az [deg]	El [deg]	Delay [nsec]	Gain [dB]
A	324.30	−0.20	29.24	−81.34
B	292.90	−0.20	38.49	−98.51
C	325.90	0.10	37.39	−97.05
D	33.10	0.60	33.19	−80.56
E	53.80	1.10	36.41	−95.11
F	0.00	0.50	54.04	−98.24
G	21.10	−0.70	55.84	−108.37
H	341.30	−0.10	57.22	−103.36
I	64.30	0.70	53.98	−101.75
J	181.70	1.50	53.81	−96.98
K	199.90	−0.70	56.98	−105.46
L	160.50	−0.30	56.59	−102.53
M	299.30	−0.30	51.03	−105.88
N	359.50	15.20	28.50	−82.63
P	359.70	−19.70	29.24	−90.80
LOS	359.60	0.20	27.57	−70.45

3.4 Analysis of H-H polarization

In the analysis of H-H polarization, Fig. 9 and 10 show the azimuth-delay power spectrum at TX and

Table 3: Parameters of the wave with the maximum power in the Rx position clusters (V-V)

Cluster	Az [deg]	El [deg]	Delay [nsec]	Gain [dB]
A	34.80	0.40	33.37	−80.59
B	31.30	−0.10	36.98	−96.11
C	66.90	0.00	38.36	−98.98
D	324.10	0.20	33.22	−80.11
E	327.70	0.30	36.50	−95.90
F	179.30	−0.10	53.73	−100.79
G	208.10	−0.40	55.49	−110.75
H	160.20	−0.10	56.90	−107.84
I	58.30	0.70	53.68	−93.39
J	0.40	0.90	54.08	−95.79
K	18.90	0.60	57.26	−106.31
L	342.10	0.00	56.88	−97.85
M	314.90	−1.60	51.52	−113.67
N	1.00	15.50	28.46	−81.61
P	359.10	−20.10	29.21	−90.38
LOS	359.10	0.20	27.54	−69.25

Table 4: Intra-cluster properties of the deterministic components derived from the Tx position (V-V)

Cluster	Az [deg]		El [deg]		Delay [nsec]		Power [dB]
⟨Waves⟩	Mean	Spread	Mean	Spread	Mean	Spread	Sum
A ⟨19⟩	323.81	3.09	−0.19	0.88	33.73	0.71	−80.17
B ⟨9⟩	283.13	15.48	−0.52	0.33	38.77	1.21	−94.26
C ⟨6⟩	336.07	6.37	0.17	0.22	38.89	1.44	−94.05
D ⟨20⟩	34.26	4.84	−0.10	0.87	33.30	0.50	−79.86
E ⟨5⟩	63.20	13.73	1.06	0.39	36.76	0.44	−92.99
F ⟨6⟩	359.37	0.71	0.88	1.61	54.17	0.35	−95.32
G ⟨3⟩	22.63	1.93	0.97	1.22	57.01	1.02	−106.05
H ⟨2⟩	341.60	0.42	0.35	0.64	57.41	0.26	−101.66
I ⟨5⟩	59.72	7.72	1.26	0.57	53.97	0.67	−99.32
J ⟨5⟩	180.43	1.91	0.75	0.79	54.00	0.23	−96.46
K ⟨1⟩	199.90	-	−0.70	-	56.98	-	−105.46
L ⟨2⟩	160.15	0.50	−0.40	0.14	56.65	0.08	−102.14
M ⟨1⟩	299.30	-	−0.30	-	51.03	-	−105.88
N ⟨25⟩	359.50	2.55	15.06	2.80	29.07	0.56	−81.45
P ⟨9⟩	359.58	0.34	−19.98	2.38	28.85	0.63	−90.26

Table 5: Intra-cluster properties of the deterministic components derived from the Rx position (V-V)

Cluster	Az [deg]		El [deg]		Delay [nsec]		Power [dB]
⟨Waves⟩	Mean	Spread	Mean	Spread	Mean	Spread	Sum
A ⟨16⟩	34.03	2.44	−0.10	1.10	33.38	0.59	−79.50
B ⟨11⟩	31.55	4.87	−0.16	1.02	37.85	1.69	−93.54
C ⟨12⟩	73.62	17.51	0.44	0.60	38.23	1.07	−92.67
D ⟨17⟩	322.08	6.73	0.10	1.04	33.65	0.71	−79.41
E ⟨8⟩	338.35	3.86	0.68	0.51	38.82	2.08	−92.83
F ⟨6⟩	181.03	5.34	0.23	0.62	53.92	0.34	−97.69
G ⟨2⟩	200.05	11.38	0.20	0.85	56.13	0.90	−109.30
H ⟨1⟩	160.20	-	−0.10	-	56.90	-	−107.84
I ⟨4⟩	50.83	5.17	−0.23	0.81	53.12	0.58	−93.26
J ⟨6⟩	0.12	1.50	0.82	1.96	54.22	0.51	−95.12
K ⟨2⟩	18.00	1.27	0.80	0.28	57.51	0.35	−104.71
L ⟨1⟩	342.10	-	0.00	-	56.88	-	−97.85
M ⟨1⟩	314.90	-	−1.60	-	51.52	-	−113.67
N ⟨21⟩	359.30	1.98	16.54	2.93	28.85	0.34	−80.29
P ⟨11⟩	359.19	0.87	-18.46	1.74	29.12	0.78	−89.87

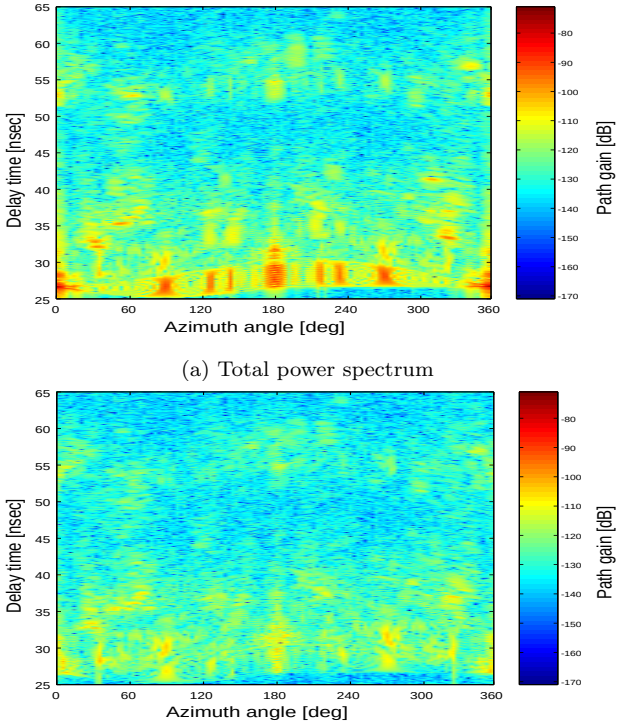

(a) Total power spectrum

(b) Residual spectrum after the extraction of 120 waves

Figure 9: Azimuth - delay power spectrum at Tx (H-H)

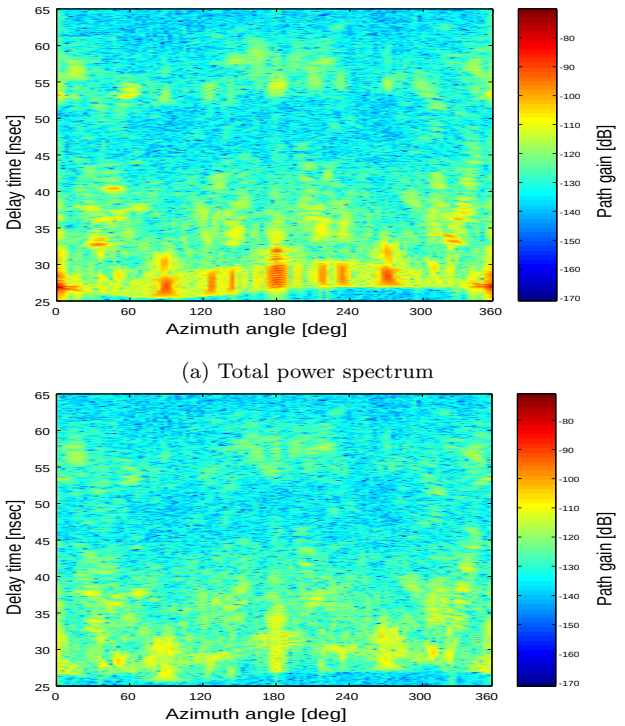

(a) Total power spectrum

(b) Residual spectrum after the extraction of 120 waves

Figure 10: Azimuth - delay power spectrum at Rx (H-H)

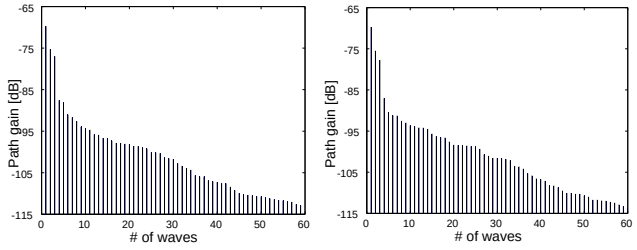

(a) Tx position (b) Rx position

Figure 11: Power of each detected wave (H-H)

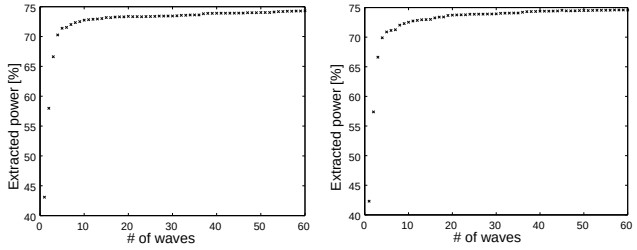

(a) Tx position (b) Rx position

Figure 12: Percentage of the sum of the extracted power (H-H)

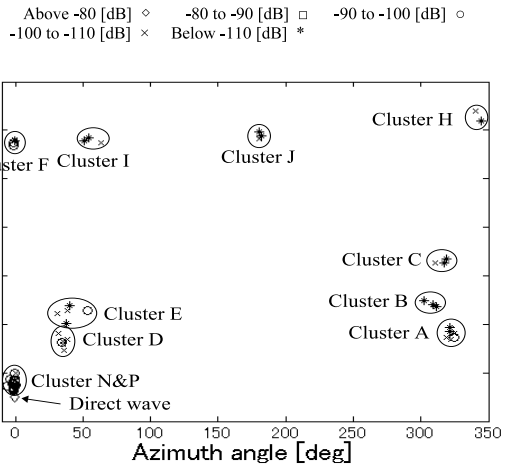

Figure 13: Clusterization of deterministic components at Tx (H-H)

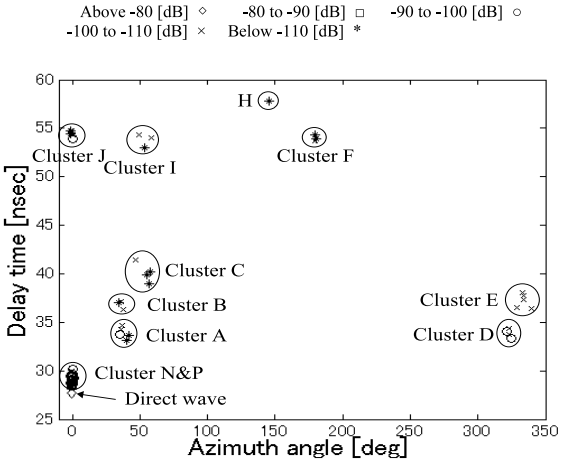

Figure 14: Clusterization of deterministic components at Rx (H-H)

Table 6: Parameters of the wave with the maximum power in the Tx position clusters (H-H)

Cluster	Az [deg]	El [deg]	Delay [nsec]	Gain [dB]
A	324.40	−0.10	33.63	−96.68
B	309.30	−0.10	37.02	−110.25
C	310.40	−0.80	41.31	−101.36
D	34.00	0.80	33.18	−96.76
E	53.20	0.00	36.38	−98.64
F	359.00	1.20	53.42	−98.16
G	-	-	-	-
H	340.10	1.30	56.99	−107.25
I	63.30	1.30	53.68	−105.94
J	180.20	−0.50	54.07	−106.89
K	-	-	-	-
L	-	-	-	-
M	-	-	-	-
N	359.10	14.00	28.41	−77.00
P	359.50	−19.00	29.17	−75.26
LOS	359.20	−0.40	27.50	−69.72

Table 7: Parameters of the wave with the maximum power in the Rx position clusters (H-H)

Cluster	Az [deg]	El [deg]	Delay [nsec]	Gain [dB]
A	35.00	1.00	33.79	−93.98
B	36.30	−0.20	37.13	−104.80
C	47.20	0.70	41.43	−100.18
D	321.20	−1.00	34.06	−97.07
E	328.80	0.50	36.52	−100.52
F	179.80	0.60	53.73	−105.32
G	-	-	-	-
H	145.00	0.40	57.81	−112.75
I	58.30	0.40	53.98	−103.13
J	0.00	1.00	53.88	−95.16
K	-	-	-	-
L	-	-	-	-
M	-	-	-	-
N	359.30	14.90	28.62	−77.22
P	359.20	−20.00	29.37	−74.99
LOS	359.30	0.60	27.72	−69.20

Table 8: Intra-cluster properties of the deterministic components derived from the Tx position (H-H)

Cluster	Az [deg]		El [deg]		Delay [nsec]		Power [dB]
⟨Waves⟩	Mean	Spread	Mean	Spread	Mean	Spread	Sum
A ⟨7⟩	322.24	1.79	−0.80	0.98	34.05	0.48	−94.25
B ⟨3⟩	307.67	4.76	1.06	0.64	37.09	0.27	−107.21
C ⟨3⟩	315.37	4.40	−0.83	0.23	41.45	0.24	−101.22
D ⟨6⟩	35.35	2.21	−0.42	0.56	33.20	0.58	−94.35
E ⟨5⟩	40.20	8.03	1.72	0.97	36.18	0.67	−97.00
F ⟨4⟩	359.25	0.26	1.00	0.96	53.78	0.26	−94.89
G ⟨-⟩	-	-	-	-	-	-	-
H ⟨2⟩	342.55	3.46	−0.45	0.47	56.49	0.71	−106.94
I ⟨3⟩	56.20	6.32	−0.33	0.09	53.92	0.25	−105.14
J ⟨3⟩	180.80	0.97	0.83	0.59	54.45	0.39	−104.91
K ⟨-⟩	-	-	-	-	-	-	-
L ⟨-⟩	-	-	-	-	-	-	-
M ⟨-⟩	-	-	-	-	-	-	-
N ⟨10⟩	359.80	1.98	16.27	2.21	28.82	0.57	−76.05
P ⟨13⟩	359.75	0.98	−18.51	2.79	29.01	0.58	−74.79

Table 9: Intra-cluster properties of the deterministic components derived from the Rx position (H-H)

Cluster	Az [deg]		El [deg]		Delay [nsec]		Power [dB]
⟨Waves⟩	Mean	Spread	Mean	Spread	Mean	Spread	Sum
A ⟨5⟩	37.88	2.87	0.24	0.59	33.88	0.60	−92.63
B ⟨3⟩	36.10	1.88	−1.47	0.11	36.82	0.44	−103.00
C ⟨4⟩	54.18	4.73	0.68	0.25	40.12	1.01	−99.98
D ⟨4⟩	323.10	1.48	0.30	0.93	33.87	0.46	−94.16
E ⟨5⟩	333.96	4.00	0.26	0.83	37.20	0.74	−97.71
F ⟨3⟩	179.83	0.35	−0.40	0.73	54.00	0.30	−103.99
G ⟨-⟩	-	-	-	-	-	-	-
H ⟨1⟩	145.20	-	0.40	-	57.81	-	−112.76
I ⟨3⟩	53.63	4.60	1.57	0.39	53.78	0.72	−102.79
J ⟨6⟩	359.45	0.70	−0.05	0.25	54.42	0.32	−94.28
K ⟨-⟩	-	-	-	-	-	-	-
L ⟨-⟩	-	-	-	-	-	-	-
M ⟨-⟩	-	-	-	-	-	-	-
N ⟨10⟩	359.82	0.78	15.29	2.64	28.85	0.48	−76.22
P ⟨16⟩	359.58	0.41	-18.91	2.94	29.12	0.53	−74.34

RX respectively. The sidelobe of the direct wave also appeared between delay time $y(25)$ to $y(30)$ at all azimuth angles. There are only 60 waves detected both at Tx and Rx position. Figure 11 shows the power of the detected waves at the Tx and Rx position. The percentage of the sum of the extracted power is 74% at both positions, even for only 60 waves. Figure 12 shows this result. For the clusterization, some clusters in Fig. 14 cannot be found as well as in V-V polarization. The properties of some clusters are also different. e.g., the power of some clusters are smaller than V-V polarization except for clusters N and P. The physical position of some clusters between V-V and H-H polarization are also a little different. This is because almost all reflective objects are positioned vertically, and the horizontal wave cross at about right angles with these reflection objects. Also, they are depended on the pattern of the antenna which is different between horizontal and vertical polarizations. Tables 6, 7, 8 and 9 show the details.

4 Conclusions

In this paper, the double-directional channel measurement and spatio-temporal analysis for UWB propagation based on the clusterization approach were reported. DoDs and DoAs are estimated separately, and are related by using high resolution ToAs and ray tracing. Double-directional channel models are prerequisites for deconvolving the antenna (Tx and Rx) transfer functions and constructing the propagation model that is independent of the antenna. Most of the clusters were determined by physical structures of the experiment environment. i.e., specular reflection, size of reflection objects, and materials. Also, the clusters were depended on the wave polarization and the pattern of antenna. Intra-cluster properties were derived based on the moment analysis, and the power, mean and spread of the DoDs, DoAs and ToAs for each cluster were shown.

References

[1] K. Haneda, and J. Takada, " An application of SAGE algorithm for UWB propagation channel estimation," in *Proc. IEEE Conf. on Ultra Wideband Systems and Technologies 2003 (UWBST2003)*, pp. 483–487, Reston, VA, USA, Nov 2003.

[2] K. Haneda, J. Takada, and T. Kobayashi, " Experimental evaluation of a SAGE algorithm for UWB channel sounding in an anechoic chamber," in *Proc. 2004 International Workshop on Ultra Wideband Systems Joint with Conference on Ultra Wideband Systems and Technologies (UWBST & IWUWBS2004)*, pp. 60–70, Kyoto, Japan, May 2004.

[3] K. Haneda, J. Takada, and T. Kobayashi, " Clusterization analysis of spatio-temporal UWB radio channel for line-of-sight and non-line-of-sight indoor home environment," accepted for *Joint COST273/284 Workshop and COST273 10th MCM*, Gothenburg, Sweden.

[4] M. Steinbauer, A. F. Molisch, and E. Bonek, " The double-directional radio channel," *IEEE Antennas and Propagat. Mag.*, Vol. 43, No. 4, pp. 51–63, Aug 2001.

[5] S. Promwong, W. Hachitani, and J. Takada, " Free space like budget evaluation of UWB-IR system, " in *Proc. 2004 International Workshop on Ultra Wideband Systems Joint with Conference on Ultra Wideband Systems and Technologies (UWBST & IWUWBS2004)*, pp. 312–316, Kyoto, Japan, May 2004.

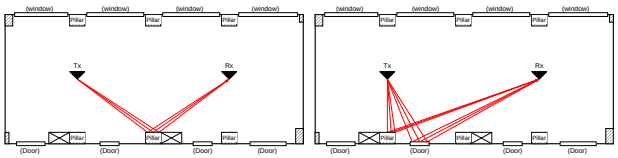

(a) Cluster A

(b) Cluster B

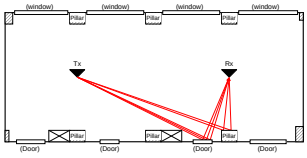

(c) Cluster C

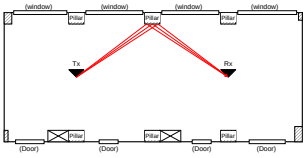

(d) Cluster D

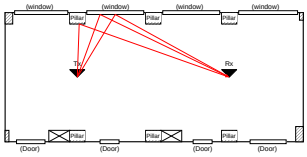

(e) Cluster E

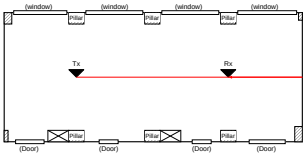

(f) Cluster F

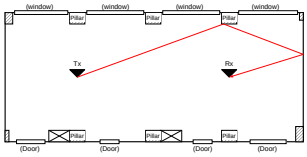

(g) Cluster G

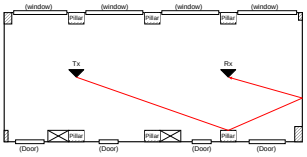

(h) Cluster H

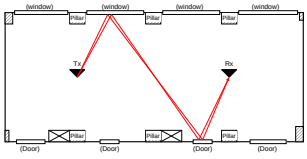

(i) Cluster I

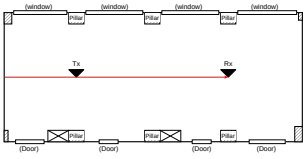

(j) Cluster J

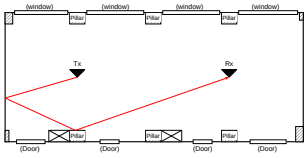

(k) Cluster K

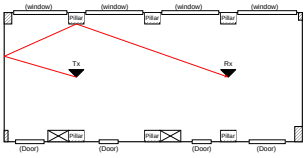

(l) Cluster L

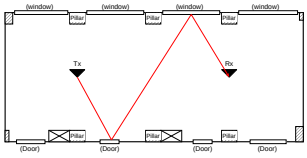

(m) Cluster M

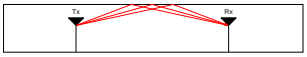

(n) Cluster N

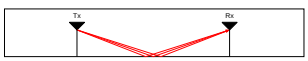

(p) Cluster P

Figure 15: Identification of clusters

[6] B. H. Fleury, X. Yin, K. G. Rohbrandt, P. Jourdan, and A. Stucki, " Performance of a high-resolution scheme for joint estimation of delay and bidirection dispersion in the radio channel," in *Proc. IEEE 55th Veicular Technology Conference (VTC 2002/Spring)*, May 2002.

[7] H. Tsuchiya, K. Haneda, and J. Takada, " Reflection and scattering analysis of Ultra Wideband indoor propagation measurements," *Technical Meeting on Instrumerntation and Measurement, IEE Japan*, IM-04-20, Jun 2004.